Since January 2020 Elsevier has created a COVID-19 resource centre with free information in English and Mandarin on the novel coronavirus COVID-19. The COVID-19 resource centre is hosted on Elsevier Connect, the company's public news and information website.

Bone 154 (2022) 116227

Contents lists available at ScienceDirect

Bone

journal homepage: www.elsevier.com/locate/bone

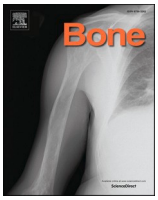

Osteoclast-mediated bone loss observed in a COVID-19 mouse model

Olatundun D. Awosanya [a,1], Christopher E. Dalloul [a,1], Rachel J. Blosser [a], Ushashi C. Dadwal [a], Mariel Carozza [b], Karen Boschen [c], Michael J. Klemsz [b], Nancy A. Johnston [c], Angela Bruzzaniti [d], Christopher M. Robinson [b], Edward F. Srour [e], Melissa A. Kacena [a,f,*]

[a] Department of Orthopaedic Surgery, Indiana University School of Medicine, Indianapolis, IN, United States
[b] Department of Microbiology and Immunology, Indiana University School of Medicine, Indianapolis, IN, United States
[c] Laboratory Animal Resource Center, Indiana University, Indianapolis, IN, United States
[d] Biomedical Sciences and Comprehensive Care, Indiana University School of Dentistry, Indianapolis, IN, United States
[e] Department of Medicine, Indiana University School of Medicine, Indianapolis, IN, United States
[f] Roudebush VA Medical Center, Indianapolis, IN, United States

ARTICLE INFO

Keywords:
SARS-CoV-2
COVID-19
Infection
Bone mass
Osteoclasts
Musculoskeletal health

ABSTRACT

The consequences of SARS-CoV-2 infection on the musculoskeletal system represent a dangerous knowledge gap. Aging patients are at added risk for SARS-CoV-2 infection; therefore, a greater understanding of the resulting musculoskeletal sequelae of SARS-CoV-2 infection may help guide clinical strategies. This study examined fundamental bone parameters among mice treated with escalating viral loads. Male C57BL/6J (WT, $n = 17$) and B6.Cg-Tg(K18-ACE2)2Prlmn/J mice (K18-hACE2 transgenic mice, $n = 21$) expressing human ACE2 (TG) were divided into eight groups ($n = 4$–6/group) and subjected to intranasal dosing of 0, 1×10^3, 1×10^4, and 1×10^5 PFU (plaque forming units) of human SARS-CoV-2. Animal health was assessed daily by veterinary staff using established and validated scoring criteria (activity, posture, body condition scores and body weight). We report here that mock and WT infected mice were healthy and completed the study, surviving until 12–14 days post infection (dpi). In contrast, the TG mice infected with 1×10^5 PFU all experienced severe health declines that necessitated early euthanasia (6–7 dpi). For TG mice infected with 1×10^4 PFU, 2 mice were also euthanized after 7 dpi, while 3 mice showed signs of moderate disease at day 6 dpi, but recovered fully by day 11 dpi. Four of the 5 TG mice that were infected with 1×10^3 PFU remained healthy throughout the study. This suggests that our study mimics what is seen during human disease, where some patients develop severe disease resulting in death, while others have moderate to severe disease but recover, and others are asymptomatic. At necropsy, femurs were extracted and analyzed by μCT. No difference was found in μCT determined bone parameters among the WT groups. There was, however, a significant 24.4% decrease in trabecular bone volume fraction ($p = 0.0009$), 19.0% decrease in trabecular number ($p = 0.004$), 6.2% decrease in trabecular thickness ($p = 0.04$), and a 9.8% increase in trabecular separation ($p = 0.04$) among surviving TG mice receiving any viral load compared to non-infected controls. No differences in cortical bone parameters were detected. TRAP staining revealed surviving infected mice had a significant 64% increase in osteoclast number, a 27% increase in osteoclast surface, and a 38% increase in osteoclasts per bone surface. While more studies are needed to investigate the long-term consequences of SARS-CoV-2 infection on skeletal health, this study demonstrates a significant reduction in several bone parameters and corresponding robust increases in osteoclast number observed within 2 weeks post-infection in surviving asymptomatic and moderately affected mice.

1. Introduction

On March 11, 2020, the World Health Organization (WHO) classified the coronavirus disease 2019 (COVID-19) as a global pandemic [1]. Initially identified in December of 2019, the race for a vaccine and fight against the virus has come a long way. However, as of September 16, 2021, despite over 5.8 billion vaccine doses administered globally, the world-wide number of confirmed cases is over 226.9 million and the

* Corresponding author at: Indiana University School of Medicine, 635 Barnhill Drive, MS549, Indianapolis, IN 46202, United States.
E-mail address: mkacena@iupui.edu (M.A. Kacena).
[1] Contributed equally to this work.

https://doi.org/10.1016/j.bone.2021.116227
Received 29 September 2021; Accepted 29 September 2021
Available online 2 October 2021

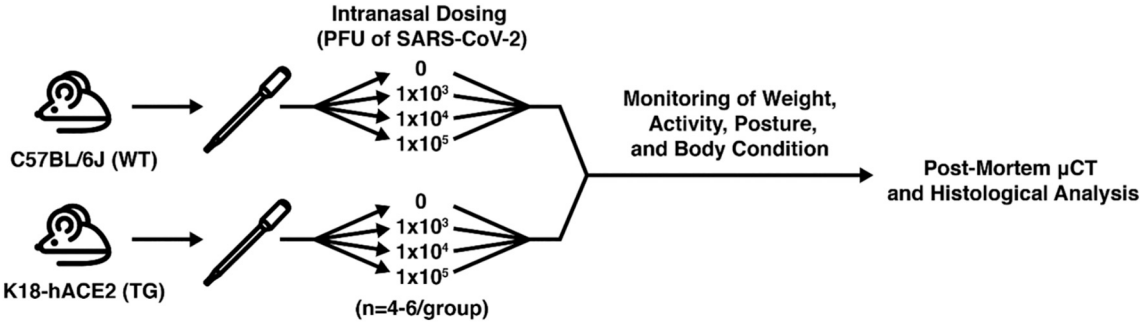

Fig. 1. Overview of experimental design. Wild-type (WT) and K18-hACE2 (TG) mice were infected with 0, 1×10^3, 1×10^4, or 1×10^5 PFU of SARS-CoV-2. Mice underwent baseline and daily health assessments and were humanely euthanized if criteria were met or were allowed to complete the entire study (12–14 days post-infection). At necropsy, femurs were collected and evaluated by μCT and histological assessments.

death count is nearing 4.7 million, with new infections occurring daily [1].

COVID-19 is caused by the novel severe acute respiratory syndrome coronavirus 2 (SARS-CoV-2). COVID-19 infection severity ranges from asymptomatic to pneumonia and acute respiratory distress syndrome (ARDS). While the pulmonary consequences are now fairly well-established given the short duration of this disease, less is known about COVID-19 infection on extra-pulmonary systems, particularly its effects on bone. Therefore, this study sought to explore fundamental bone micro-structural and histomorphometric parameters in a mouse model of COVID-19 infection.

There are several mechanisms through which SARS-CoV-2 may impact the skeletal system. For example, human angiotensin-converting enzyme 2 (hACE2), which SARS-CoV-2 utilizes as its entry receptor, is expressed in cortical and trabecular bone [2,3]. Additionally, many inflammatory cytokines upregulated in the cytokine storm associated with COVID-19 infection have well-established roles in osteoclastogenesis and/or low bone mineral density including: IL-1β, IL-6, IL-17, CXCL10, and TNF-α [3–8]. Further, hypocalcemia is common among COVID-19 patients and can be used to predict disease severity [9].

B6.Cg-Tg(K18-ACE2)2Prlmn/J mice (K18-hACE2 transgenic mice [TG], Jackson Laboratory) serve as an excellent model for COVID-19 because it uses the unaltered human virus [10–12]. As most variants of SARS-CoV-2 are unable to effectively infect mice expressing mouse ACE2 [13], these mice express human ACE2 (hACE2) driven by the cytokeratin 18 promoter resulting in hACE2 expression in airway, liver, kidney, and gastrointestinal epithelial cells [14–16]. K18-hACE2 mice are susceptible to SARS-CoV-2, and intranasal inoculation can result in severe disease that mimics the severe form of the human disease, including interstitial pneumonia and pulmonary pathology, and upregulation of proinflammatory cytokines [17,18]. In the current study, we investigated the consequences of SARS-CoV-2 infection on the skeletal system of K18-hACE2 mice.

2. Materials and methods

2.1. COVID-19 mouse model

All animal studies were approved by the Indiana University School of Medicine Institutional Animal Care and Use Committee (IACUC) as well as the Indiana University Institutional Biosafety Committee (IBC). Male B6.Cg-Tg(K18-ACE2)2Prlmn/J mice (Jackson Laboratory, Bar Harbor, ME, Stock No: 034860) were used in these studies. From hereon, K18-hACE2 transgenic mice will be referred to as TG mice. Hemizygous TG mice were bred with C57BL/6 J mice (Jackson Laboratory, Stock No: 000664) to generate wild-type (WT) and TG littermates that were used in these studies.

At approximately 19 weeks of age, 17 male WT and 21 male TG mice were either mock infected (media only) or were infected (media containing virus) intranasally (50 μl) with SARS-CoV-2 isolate USA-WA1/2020 (BEI Resources, Manassas, VA), $n = 4$–6/group using methods described by Santry et al. [19] Mice were administered a viral concentration of 0 (mock), 1×10^3, 1×10^4, or 1×10^5 PFU (plaque-forming unit). Mice were weighed at baseline and daily post-infection. Several additional assessments were also completed each day including: body weight, activity score, posture score, and body condition score (BCS) as detailed below. Fig. 1 provides an overview of our experimental design.

Table 1
Activity scores.

Score	Activity
0	Normal
1	Slightly reduced/mild gait abnormality
2	Moving very slowly/severely altered gait
3	Reluctant to move or did not move

2.2. Virus preparation

Vero-furin cells were grown in Dulbecco's modified Eagle's medium (DMEM) supplemented with 10% fetal bovine serum and 1% penicillin-streptomycin at 37 °C with 5% CO_2. SARS-CoV-2 isolate USA-WA1/2020 was propagated in Vero-furin cells and progeny virions were collected in the supernatant 2–3 days post-infection. SARS-CoV-2 was quantified by a plaque assay in Vero-furin as previously described [20].

2.3. Activity scoring

Mice were assessed for activity level daily via cageside observation. The activity score was based on the degree of movement by the mice in the cage and gait as previously described [21–23]. As shown in Table 1, a score of 0 indicated normal activity and that mice were bright and alert. A score of 1 indicated slightly reduced activity or mild gait abnormality. A score of 2 indicated the very slow movement or a severely altered gait. A score of 3 indicated that movement was reluctant or did not take place at all.

Table 2
Posture scores.

Score	Posture
0	Normal
1	Slightly hunched
2	Moderately hunched
3	Severely hunched

Table 3
Body condition scores.

Score	Body condition score (BCS)
1	Emaciated/severe muscular wasting
2	Underconditioned/modest muscular wasting
3	Normal
4	Overconditioned/well-fleshed
5	Obese

Table 4
Mice with total scores of 5–6 (activity score + posture score) were euthanized or if a loss of more than 15% of the baseline body weight was observed in 2 consecutive measurements.

Score	Activity	Posture
0	Normal	Normal
1	Slightly reduced/mild gait abnormality	Slightly hunched
2	Moving very slowly/severely altered gait	Moderately hunched
3	Reluctant to move or did not move	Severely hunched
	Activity range [0–3]	Posture range [0–3]

Total score: activity + posture [range: 0–6].

Table 5
Mice with scores of 5–6 (modified BCS + modified weight) were euthanized if activity score from daily assessments was ≥2 on 2 consecutive days.

Score	Body condition score (BCS)	Weight
0	BCS 3	Normal (at baseline)
1	BCS 2.9–2.5	loss of up to 10% of baseline weight
2	BCS 2.4–2.0	loss of 10%–15% of baseline weight
3	BCS less 1.9	loss of more than 15% of baseline weight
	BSC range [0–3]	Weight range [0–3]

Total score: BCS + weight [range: 0–6].

2.4. Posture scoring

Mice were also assessed for posture through daily cageside observation. Posture scoring was assessed on a 0–3 range as previously detailed [21]. As shown in Table 2, a score of 0 was the baseline and represented normal posture. A score of 1 represented a slightly hunched posture in a mouse. A score of 2 indicated a mouse was moderately hunched. A score of 3 indicated a mouse was severely hunched.

2.5. Body condition scoring

Body condition scores (BCS) were performed as previously described [24] and ranged from 1 to 5. As detailed in Table 3, the baseline or normal score is 3. A score of 4 represents an overconditioned and fleshy mouse. A score of 5 is an obese mouse. On the other hand, a score of 2 represents an underconditioned mouse showing signs of muscular wasting. A score of 1 represents an emaciated mouse with severe muscular wasting.

2.6. Criteria for humane euthanasia

Criteria for humane endpoints were established in consultation with IACUC and collaborating veterinarians. As described above, mice were observed daily for changes in activity, posture, body condition, and weight. The following combined measures triggered humane euthanasia. 1) Mice with a combined score for activity + posture equaling 5–6 (see Table 4). 2) Mice with a combined score for modified BCS + weight loss equaling 5–6 along with a ≥2 activity score for 2 consecutive days (see Table 5). 3) Mice with more than a 15% decline in body weight from baseline on 2 consecutive days. The scoring system above was developed with the goal of identifying mice that would likely die within 24 h, allowing for the timely and humane euthanization of very sick animals.

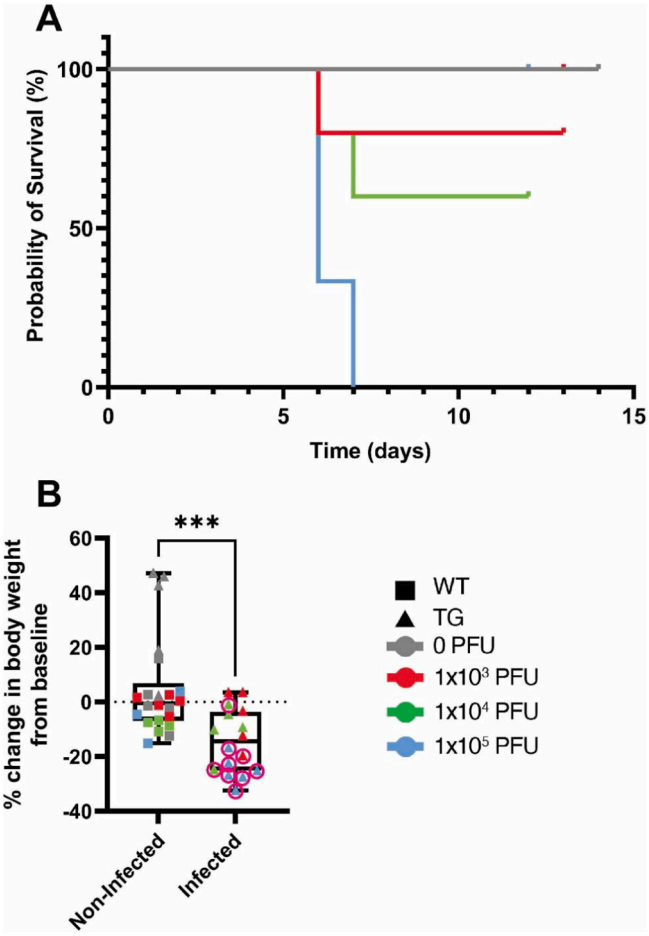

Fig. 2. Effects of SARS-CoV-2 infection on survival and body weights in mice. C57BL/6J (WT) and K18-hACE2 (TG) mice were infected with 0, 1×10^3, 1×10^4, or 1×10^5 PFU of SARS-CoV-2 and survival (A) and the percent change in body weight at euthanasia from baseline (B) were assessed at baseline and daily until humane euthanasia occurred or 12–14 days post infection (n = 4–6/genotype/viral load). A) Kaplan-Meier survival curves. It should be noted that all WT mice (0, 1×10^3, 1×10^4, or 1×10^5 PFU) and TG mice infected with 0 PFU survived for the entire study and are overlapping the gray line at 100%. Different colored lines represent the different viral infection doses (gray = 0 PFU, red = 1×10^3 PFU, green = 1×10^4 PFU, blue = 1×10^5 PFU). B) Percent change in body weight at the time of euthanasia from baseline body weight measurements for non-infected (n = 22) and infected mice (n = 16). Data from individual mice are shown. ***$p < 0.005$ compared to non-infected mice. Statistical analysis was performed using a Student's t-test. (For interpretation of the references to colour in this figure legend, the reader is referred to the web version of this article.)

We believe that this system allowed us to predict death with accuracy. As some animals will recover after infection, this would also allow us to differentiate between those two populations.

2.7. Micro-computed tomography

At the time of euthanasia the right femur was dissected, stripped of soft tissue, and fixed in 10% neutral buffered formalin (NBF) for 3 days. Femurs were then transferred to 70% ethanol (EtOH) where they remained until processing for histological analyses as detailed below. Prior to histological processing femurs were imaged using a desktop SkyScan 1172 μCT imaging system (SkyScan, Kontich, Germany) with a 9.8 μm voxel size, 59 kV voltage, 167 μA current, and a 0.5-mm-thick aluminum filter. Image reconstructions were obtained via NRecon v.1.7.3 using a ring artifact correction of 5 and a beam hardening

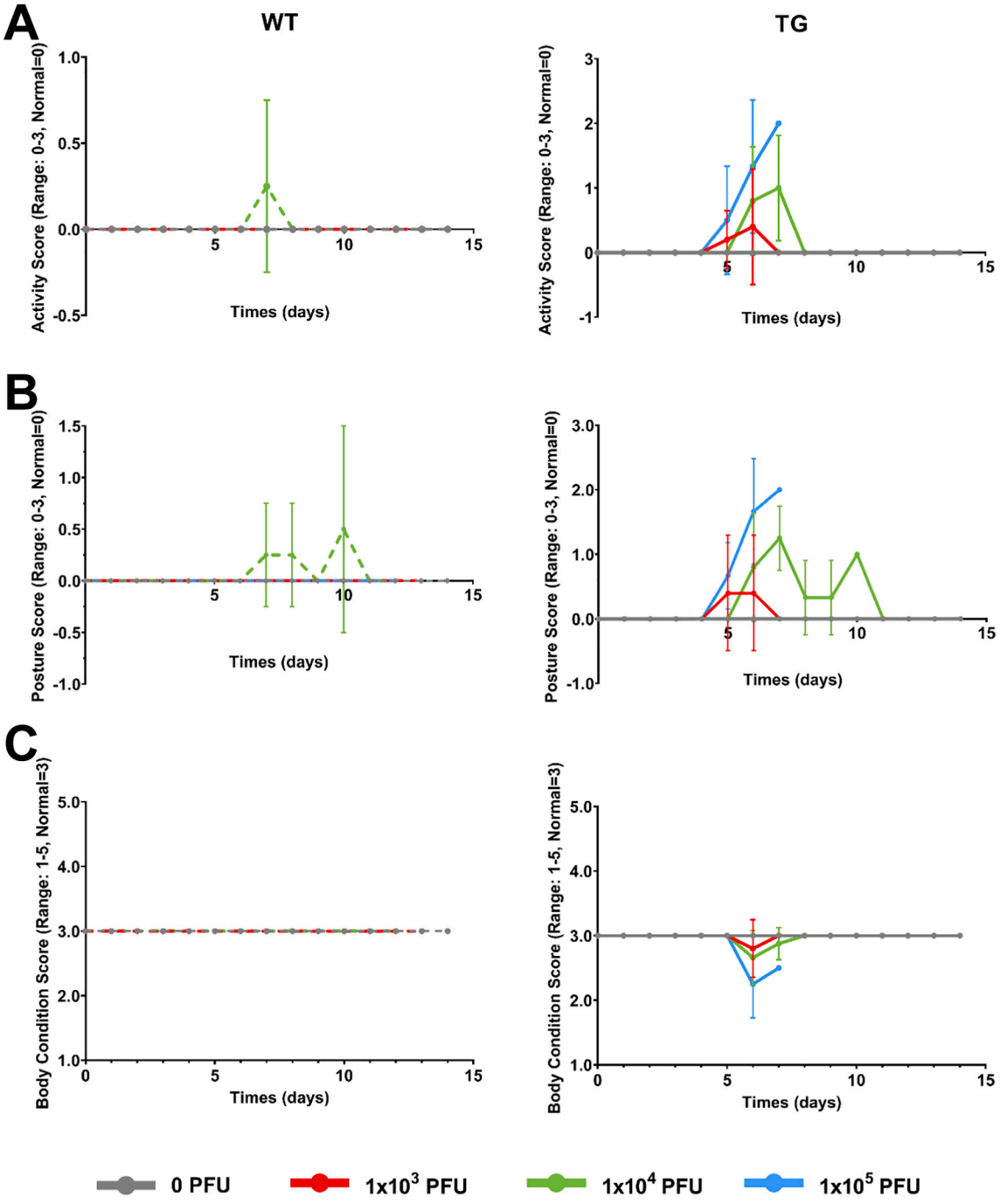

Fig. 3. Effects of SARS-CoV-2 infection on activity, posture, and body condition scores in mice. C57BL/6 J (WT) and K18-hACE2 (TG) mice were infected with 0, 1×10^3, 1×10^4, or 1×10^5 PFU of SARS-CoV-2 and several common, validated veterinary health measures were scored at baseline and daily until humane euthanasia occurred or 12–14 days post infection (n = 4–6/genotype/viral load). A) Average activity score (range 0–3, normal = 0). B) Average posture score (range 0–3, normal = 0). C) Average body condition score (range 1–5, normal = 3). Data are presented as the mean ± standard deviation. Dashed lines represent WT mice and solid lines represent TG mice. Different colored lines represent the different viral infection doses gray = 0 PFU, red = 1×10^3 PFU, green = 1×10^4 PFU, blue = 1×10^5 PFU). Note, activity and posture scores increase from 0 when mice exhibit declines in health, whereas BCS drops below 3 when mice are underconditioned or rises above 3 when mice are overconditioned. (For interpretation of the references to colour in this figure legend, the reader is referred to the web version of this article.)

correction of 20%. The volume of interest (VOI) for metaphyseal analysis started 75 slices (or 0.738 mm) proximal to the distal growth plate and extended 100 slices (total of 0.983 mm) proximally. The trabecular and cortical bone were automatically segmented from each other using a custom task-list. The VOI for diaphyseal analysis was a 200-slice (total of 1.966 mm) region centered at half the distance from the distal condyle to the proximal point of the femoral head.

2.8. Histology and histomorphometry

After being scanned, femurs were decalcified in Immunocal Decalcifier (Statlab, Mckinney, TX) for 48 h, processed, and embedded in paraffin. Femora were then cut into 5-μm-thick sections in the sagittal plane and mounted on glass slides. Slides were stained with tartrate resistant acid phosphatase (TRAP). Images were captured at 20×

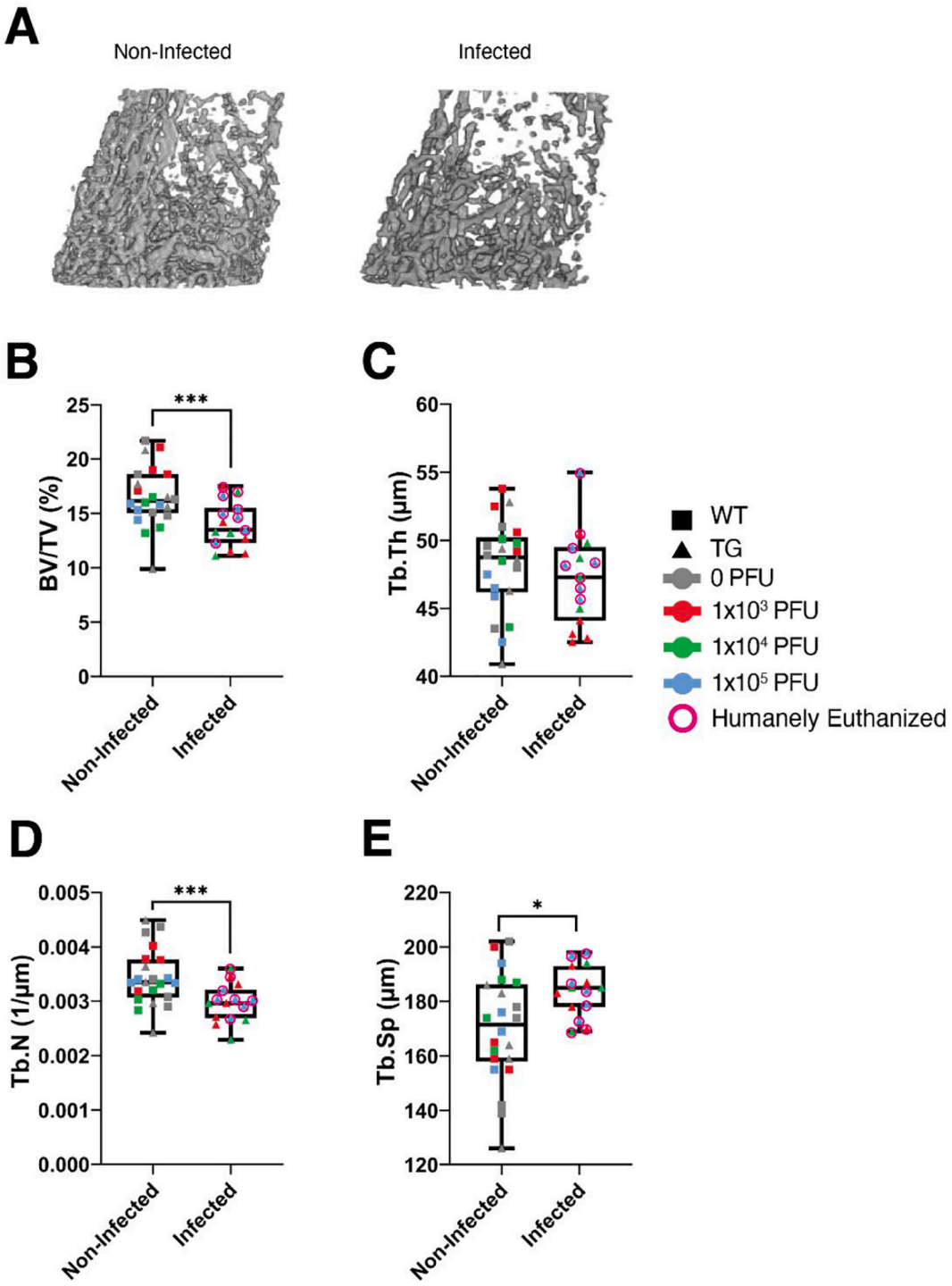

Fig. 4. Effects of SARS-CoV-2 infection on trabecular bone parameters in mice. C57BL/6J (WT) and K18-hACE2 (TG) mice were infected with 0, 1×10^3, 1×10^4, or 1×10^5 PFU of SARS-CoV-2. Non-infected mice included mock-infected (0 PFU) TG mice and all WT mice (infected with 0, 1×10^3, 1×10^4, or 1×10^5 PFU) ($n = 22$). Infected mice included TG mice infected with 1×10^3, 1×10^4, or 1×10^5 PFU of SARS-CoV-2 virus ($n = 15$, due to a femur being broken during removal from a TG mouse infected with 1×10^4 PFU, early endpoint). A) Representative μCT images of the distal metaphyseal femur of surviving TG mice infected with 0 and 1×10^4 PFU. B–E) Quantitative microstructural parameters determined by μCT. B) Bone volume fraction (BV/TV). C) Trabecular thickness (Tb.Th). D) Trabecular number (Tb.N). E) Trabecular separation (Tb.S). Data are presented as the mean ± standard deviation. Mice which were humanely euthanized prior to the study endpoint are denoted by pink circles. $^*p < 0.05$ and $^{***}p < 0.005$ compared to non-infected mice. Statistical analysis was performed using a Student's *t*-test. (For interpretation of the references to colour in this figure legend, the reader is referred to the web version of this article.)

magnification using a Leica DM2700 M microscope (Leica Microsystems, Buffalo Grove, IL). Histomorphometric parameters were determined in an area 1000 pixels proximal to the growth plate with a 75-pixel border in a semi-automated manner using Bioquant OSTEO (Bioquant Image Analysis Co., Nashville, TN).

2.9. Statistical analysis

Statistical analyses were performed with GraphPad Prism (ver. 8, GraphPad Software, La Jolla, CA). Results are displayed as mean ± SD. To compare two groups, a two-tailed Student's *t*-test was used. To

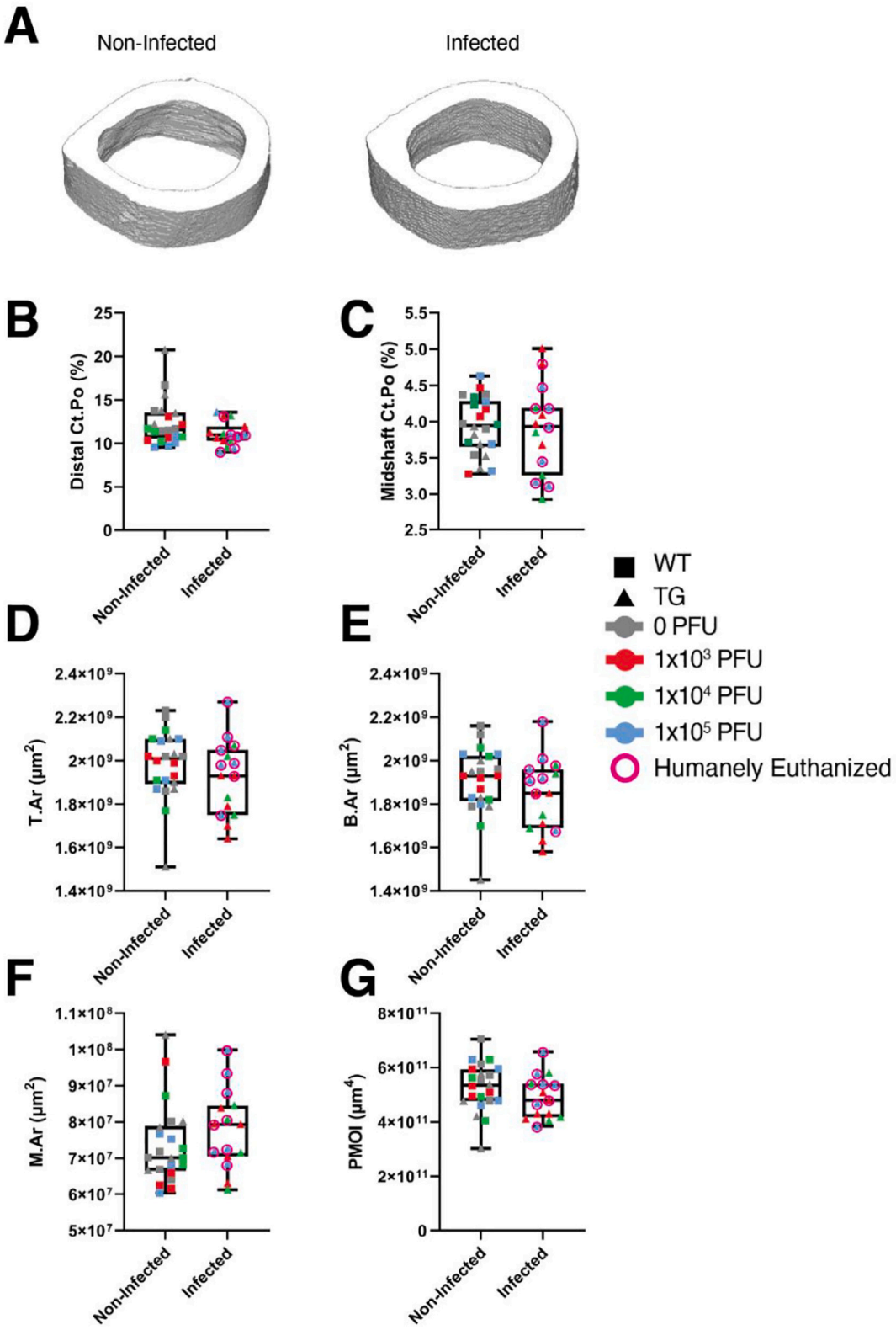

Fig. 5. SARS-CoV-2 infection does not impact cortical bone parameters. C57BL/6J (WT) and K18-hACE2 (TG) mice were infected with 0, 1×10^3, 1×10^4, or 1×10^5 PFU of SARS-CoV-2. Non-infected mice included mock-infected (0 PFU) TG mice and all WT mice (infected with 0, 1×10^3, 1×10^4, or 1×10^5 PFU) ($n = 22$). Infected mice included TG mice infected with 1×10^3, 1×10^4, or 1×10^5 PFU of SARS-CoV-2 virus ($n = 15$, due to a femur being broken during removal from a TG mouse infected with 1×10^4 PFU, early endpoint). A) Representative μCT images of the cross-sectional area at the midshaft of the femur of surviving TG mice infected with 0 and 1×10^4 PFU. B–G) Quantitative microstructural parameters determined by μCT. B) Cortical bone porosity (Ct.Po, distal). C) Cortical bone porosity (Ct.Po, midshaft). D) Tissue area (T.Ar, midshaft). E) Bone area (B.Ar, midshaft). F) Marrow area (M.Ar, midshaft). G) Polar moment of intertia (PMOI, midshaft). Data are presented as the mean ± standard deviation. Mice which were humanely euthanized prior to the study endpoint are denoted by pink circles. No significant differences were detected. Statistical analysis was performed using a Student's *t*-test. (For interpretation of the references to colour in this figure legend, the reader is referred to the web version of this article.)

compare three or more groups, a one-way ANOVA with Tukey-Kramer post hoc test was performed. p-Values < 0.05 were considered significant.

3. Results

3.1. Survival and overall health of infected mice

WT and TG mice were infected with 0, 1×10^3, 1×10^4, or 1×10^5 PFU of SARS-CoV-2 ($n = 4$–6/group), as has been previously described [12,16,25]. All WT mice (mock-infected or infected) survived and were healthy for the study duration (12–14 days post-infection (dpi), Figs. 2 and 3). Specifically, no significant differences in these mice from baseline were observed in any of the parameters examined. As also illustrated in Figs. 2 and 3, all TG mock-infected mice (gray solid line) survived and were healthy with no significant differences in body weight (percent change from baseline), activity scores, posture scores, or BCS. Taken together, all of these control, "non-infected" mice exhibited very similar health and behavior traits with no clinical signs of illness observed throughout the study.

Next, we examined the survival and health characteristics of infected TG mice. Consistent with other studies, [12,16,25] as illustrated in Fig. 2A (blue line), all TG mice infected with 1×10^5 PFU required humane euthanasia at 6–7 dpi based on veterinarian approved assessment of poor health (described in Tables 4 and 5 above). These deteriorating health characteristics can be visualized in Figs. 2B and 3A–C (note the worsening trend of the blue line or symbol e.g. that the blue line is far from the baseline and mock-infected control gray line). It is important to keep in mind that the validated activity and posture scores increase from 0 when mice exhibit declines in health, whereas the validated BCS drops below 3 when the mice are underconditioned or show signs of muscular wasting. As illustrated in Figs. 2 and 3, in general TG mice receiving 1×10^3 PFU (red line) appeared healthy, except one mouse which was humanely euthanized at 6 dpi. Surviving mice infected with 1×10^3 PFU showed no significant clinical differences in health parameters tested throughout the entire study, compared to TG mock-infected and WT controls (see red line/symbol compared to gray line/symbol in Figs. 2 and 3). As shown in Figs. 2 and 3, although two K18-hACE2 mice receiving 1×10^4 PFU (green line/symbol) were humanely euthanized at 7 dpi, the remainder of the cohort showed an initial decline in health assessment parameters, but recovered fully, and by 11 dpi, showed no differences in terms of percent change in body weights, activity scores, posture scores, and BCS, compared to control mice and baseline values.

Regarding the presentation of data figures from Fig. 2B onward, for ease of presentation, mice have been combined into 2 groups: "non-infected mice" (all WT mice and TG mice infected with 0 PFU) and "infected mice" (all TG mice infected with any viral dose, those that died and survived). For the remainder of the figures, squares represent WT mice and triangles represent TG mice. Gray lines/symbols represent mice infected with 0 PFU, red lines/symbols = 1×10^3 PFU, green lines/symbols = 1×10^4 PFU, and blue lines/symbols = 1×10^5 PFU. A pink circle around a triangle indicates when a mouse was humanely euthanized prior to the endpoint of the study. Therefore a red square represents a WT mouse infected with 1×10^3 PFU of SARS-CoV-2, while a green triangle with a pink circle around it represents a TG mouse infected with 1×10^4 PFU of SARS-CoV-2 that had to be humanely euthanized before the study endpoint.

With respect to the percent change from baseline in body weight at the time of euthanasia, as shown in Fig. 2B, collectively, infected mice exhibited a significant 14.3% reduction in body weight compared to the 4.9% increase in body weight observed in non-infected mice ($p = 0.0008$). As shown in Fig. 2B, the majority of the mice that were euthanized prior to the study endpoint exhibited larger changes in body weight than that observed in those that survived. Indeed, comparing non-infected mice to those that were euthanized prior to the study endpoint showed a significant 21.8% reduction in body weight ($p = 0.0003$), whereas comparing non-infected mice to those that survived to the study endpoint showed no significant difference in body weight change ($p = 0.2$). Overall this suggests that surviving infected mice exhibit body weight changes that were not significantly different from non-infected controls, while infected mice with severe illness requiring early humane euthanasia experienced significant reductions in body weight.

3.2. Significant trabecular bone loss in surviving TG mice infected with SARS-CoV-2

A primary goal of this study was to examine whether infection with SARS-CoV-2 resulted in changes in bone parameters. Following euthanasia, femurs were collected and μCT analysis was completed. To examine whether mice with SARS-CoV-2 infection had different trabecular bone parameters compared to mice which were not infected, we combined the mice as detailed above. Briefly, infected mice were TG mice infected with 1×10^3, 1×10^4, or 1×10^5 PFU of SARS-CoV-2 virus, and non-infected mice were mock-infected (0 PFU) TG mice as well as all WT mice (infected with 0, 1×10^3, 1×10^4, or 1×10^5 PFU of SARS-CoV-2 virus). Fig. 4A shows representative μCT images of the trabecular bone within the distal metaphyseal region of femurs from non-infected and infected mice used for these analyses. As detailed in Fig. 4B, TG mice receiving any amount of virus (infected mice) showed a significant decrease in trabecular bone volume fraction (BV/TV) compared to non-infected mice (−15.4%, $p = 0.004$). Although a significant difference in BV/TV was detected when all infected mice are grouped together and compared to all non-infected mice, mice that were euthanized at 6–7 dpi did not show a reduction in bone mass (BV/TV: −7.6%, $p = 0.2$), whereas infected mice that survived to the study endpoint (12–14 dpi) showed a significant reduction in bone mass (BV/TV: −24.4%, $p = 0.0009$). This suggests that bone loss is likely occurring during the latter stages of infection.

When examining the parameters associated with the reduction in BV/TV, as shown in Fig. 4C, no significant difference was detected in trabecular thickness (Tb.Th) when all infected TG mice were compared to all non-infected mice ($p = 0.4$). However, when comparing infected mice that survived to the study endpoint compared with those that did not survive, it was determined that surviving mice exhibited a significant reduction in Tb.Th (−6.2%, $p = 0.04$), whereas mice humanely euthanized did not exhibit a change in Tb.Th (+1.5%, $p = 0.6$), compared to all non-infected mice. With regard to trabecular number (Tb.N), as illustrated in Fig. 4D, combined all infected TG mice had a significant reduction in Tb.N compared to all non-infected mice (−13.7%, $p = 0.004$). Surviving mice exhibited a significant reduction in Tb.N (−19.0%, $p = 0.004$), while mice euthanized 6–7 dpi exhibited no change inTb.N (−9.0%, $p = 0.1$) compared to all non-infected mice. Finally, with respect to trabecular separation (Tb.Sp), as shown in Fig. 4E, combined all infected TG mice experienced a significant increase in Tb.Sp compared to non-infected controls (+8.5%, $p = 0.01$). For Tb.Sp, surviving mice showed a significant increase (+9.8% $p = 0.03$), but mice euthanized 6–7 dpi showed a non-significant increase (+7.2% $p = 0.1$) compared to non-infected mice.

3.3. SARS-CoV-2 does not change cortical bone properties in mice

We then examined whether SARS-CoV-2 infection resulted in changes to cortical bone parameters. Femoral cortical porosity was examined at both the distal metaphyseal region and the diaphyseal midshaft. No significant differences were observed between infected and non-infected mice in either bone region (Fig. 5). We also found no significant differences among any groups with respect to the midshaft tissue area (T.Ar), bone area (B·Ar), marrow area (M.Ar), and polar moment of inertia (PMOI) (Fig. 5).

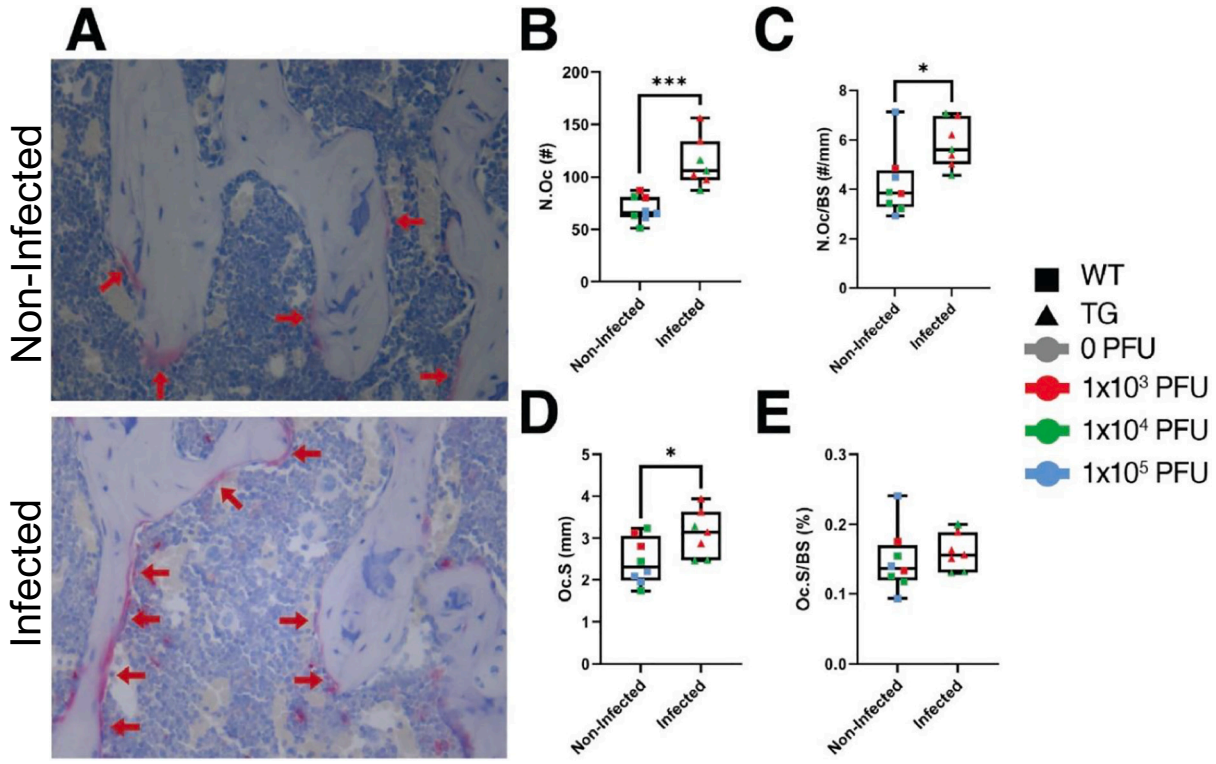

Fig. 6. Osteoclast parameters are elevated in mice infected with SARS-CoV-2. A) Representative micrographs of TRAP staining in femurs from non-infected ($n = 8$) and infected mice ($n = 7$). Osteoclasts stain red (red arrows). Quantitation of B) Number of osteoclasts (N.Oc); C) number of osteoclasts per bone surface (N.Oc/BS); D) osteoclast surface (Oc.S); and E) osteoclast surface per bone surface (Oc.S/BS). $^{*}p < 0.05$ or $^{***}p < 0.005$ compared to non-infected mice. Statistical analysis was performed using a Student's *t*-test. (For interpretation of the references to colour in this figure legend, the reader is referred to the web version of this article.)

3.4. Increases in osteoclasts observed in TG mice infected with SARS-CoV-2

Following μCT scanning, a subset of femurs from mice which survived to the study endpoint were subjected to demineralization, paraffin embedding, sectioning, and TRAP staining. As above, histological specimens were divided into 2 groups: non-infected ($n = 8$) or infected mice ($n = 7$). As shown in Fig. 6A, significantly more TRAP+ osteoclasts were observed in histological sections from femurs of infected mice than were observed in femurs from non-infected mice. These observations were quantitated (Fig. 6B–E) and it was determined that there was a significant 64.3% increase in the number of osteoclasts (N.Oc, $p = 0.0004$), a significant 38.1% increase in the number of osteoclasts per bone surface (N.Oc/BS, $p = 0.02$), a significant 27.2% increase in osteoclast surface (Oc.S, $p = 0.04$), but a non-significant 8.5% increase in the osteoclast surface per bone surface (Oc.S/BS, $p = 0.5$).

4. Discussion

Here we report that in a mouse model of COVID-19, infection of K18-hACE2 TG mice with SARS-CoV-2 represents 3 important classes of COVID patients: those who die (1×10^5 PFU), those with moderate to severe disease who may recover (1×10^4 PFU), and those who are asymptomatic (1×10^3 PFU). All of the infected TG mice experienced a robust loss of trabecular bone volume fraction (Fig. 4), likely owing to the significant 64% increase in TRAP+ osteoclasts (Fig. 6). Importantly, when we examined only mice that survived to the study endpoint (approximately 1 week longer survival duration), an even more dramatic change in trabecular bone parameters was observed. While additional studies would be required to test this idea, it is not an unreasonable hypothesis as it takes time for new osteoclasts to form and begin breaking down bone.

Another important observation is that the bone loss observed following SARS-CoV-2 infection occurs even in the surviving TG mice infected with 1×10^3 PFU, which had no clinical signs of illness as assessed by measuring changes in body weights, activity scores, posture scores, and BCS (Figs. 2 and 3). The finding that all surviving mice in the 1×10^3 PFU group were as active as the controls, is important as if a mouse is sick and not moving, we may expect significant bone loss. Indeed, perhaps the most dramatic case scenario for inactivity and lack of mobility would be with unloading such as that observed with spaceflight or hindlimb unloading. In a hindlimb unloading study completed in the same background strain of mice at approximately the same age for the same study duration (4 month old C57BL/6 mice subjected to 2 weeks of unloading) investigators observed a 22% reduction in distal femur bone volume fraction [26]. In comparison, our surviving TG mice infected with 1×10^3 PFU of SARS-CoV-2 experienced a 25% reduction in distal femur bone volume fraction and remained load bearing throughout the study.

Although limitations of our study include low sample size ($n = 4$–6/genotype/viral dose), only one sex (male), and one age (approximately 19 weeks at the time of infection), as we are still in the midst of the COVID-19 pandemic, it was important to report on a statistically sound observation that has not been yet examined as a sequalae of this disease. This is especially true because as of September 16, 2021 the number of confirmed COVID-19+ cases reached over 226.9 million, while the death count was nearly 4.7 million [1]. Thus, there are millions of people who have already suffered from COVID-19 and bone loss may be yet another critically important secondary complication associated with having been infected with SARS-CoV-2.

Bone loss is a common side effect of aging and post-menopausal osteoporosis. Indeed, studies demonstrate that approximately 1 in 2 women, and 1 in 4 men over the age of 50 will suffer a fractured bone as a result of osteoporosis [27]. Therefore, it is formally possible that those

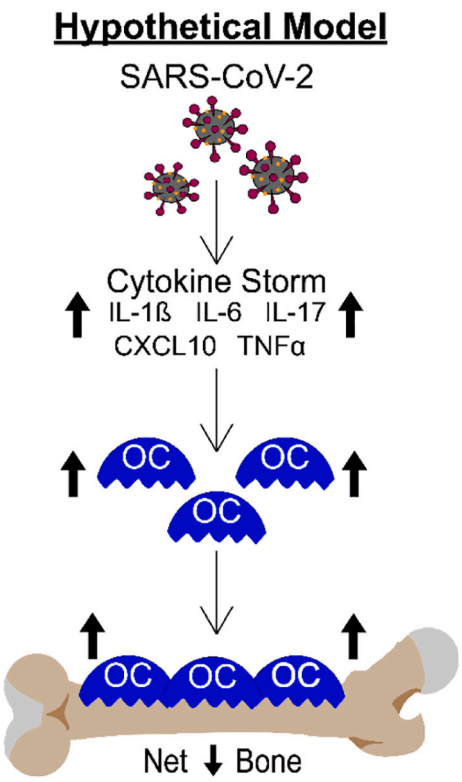

Fig. 7. Schematic demonstrating our hypothetical model describing how the cytokine storm associated with SARS-CoV-2 infection may result in osteoclast-mediated bone loss.

who contracted COVID-19 may be more likely to be diagnosed with osteoporosis and/or may be at higher risk of developing fractures. However, it is important to note that these studies do not demonstrate whether the bone loss observed can be recovered over time. While it would be important to determine this for all individuals, it may be particularly important to understand this for the aged population, where they are already at risk for age-associated osteoporosis.

It is critically important to understand the long-term consequences of this dramatic bone loss. However, it is equally important to understand the mechanisms of action. While not specifically tested in this study, it is well known that patients with severe forms of COVID-19 have upregulated expression of numerous cytokines and growth factors which together lead to the inflammatory "cytokine storm" [28–33]. Many of these cytokines, including IL-1β, IL-6, IL-17, CXCL10, and TNF-α are known to regulate osteoclastogenesis and/or bone resorption [3–8], suggesting these factors may contribute to the SARS-CoV-2 stimulated bone loss observed in our K18-hACE2 mouse model. Fig. 7 shows a working model of how SARS-CoV-2 infection may be regulating osteoclast-mediated bone loss.

We recognize that the cytokine storm is just one possible mechanism by which bone loss occurs and much more work is needed to fully elucidate the mechanisms of action. For example, a recent study found that SARS-CoV-2 could directly infect bone marrow macrophages to a higher extent than mature osteoclasts [34]. Further, their study suggests that infection may alter the ability of bone marrow macrophages to differentiate into osteoclasts. Regardless of the mechanism of action, infection with SARS-CoV-2 results in a dramatic upregulation in osteoclastogenesis and a robust loss of bone within 2 weeks post-infection in a COVID-19 mouse model. Whether these findings translate into humans remains to be determined, but if they do, an increase in fractures may be observed secondary to COVID-19 disease in the not too distant future.

CRediT authorship contribution statement

Conception and Design of the Study: MJK, NAJ, EFS, and MAK conceived and designed the study. Acquisition of Data: ODA, CED, RJB, UCD, MC, KB, NAJ, and MAK primarily conducted the experiments. Data Analysis and Interpretation: All authors contributed to the data analysis and interpretation. Data interpretation: All authors provided interpretation of various results. Drafting Manuscript: ODA, CED, NAJ, and MAK, with input from all co-authors, wrote the draft of the manuscript. Revising Manuscript for Important Intellectual Content: All authors critically revised the manuscript. Approval of the Final Content of the Manuscript: All author approved the final content of the manuscript.

Acknowledgements

We would like to thank Ms. Jennifer Sickles and Ms. Chelsea Roberts for their assistance with caring for the mice. This project was supported, in part, by the Cooperative Center of Excellence in Hematology (CCEH) Award, funded in part by NIH 1U54DK106846 (MAK, EFS, UCD); the Indiana Clinical and Translational Sciences Institute, funded in part by NIH UL1TR002529 (MAK), NIH T32 DK007519 (UCD), NIH T32 AR065971 (UCD), and NIH T32 HL007910 (ODA). In addition, the results of this work were supported with resources and the use of facilities at the Richard L. Roudebush VA Medical Center, Indianapolis, IN: VA Merit #BX003751 (MAK). We would also like to thank the Histology and Histomorphometry Core (Indiana Center for Musculoskeletal Health) for assistance with processing and staining of histological specimens. Finally, the views expressed in this article are solely those of the authors and do not necessarily represent the official position or policy of any of the aforementioned agencies.

References

[1] E. Dong, H. Du, L. Gardner, An interactive web-based dashboard to track COVID-19 in real time, Lancet Infect. Dis. 20 (5) (2020) 533–534.
[2] N. Zamorano Cuervo, N. Grandvaux, ACE2: evidence of role as entry receptor for SARS-CoV-2 and implications in comorbidities, eLife. (2020) 9.
[3] N.P. Disser, A.J. De Micheli, M.M. Schonk, et al., Musculoskeletal consequences of COVID-19, J. Bone Joint Surg. 102 (14) (2020) 1197–1204.
[4] L. Gilbert, X. He, P. Farmer, et al., Inhibition of osteoblast differentiation by tumor necrosis factor-α, Endocrinology. 141 (11) (2000) 3956–3964.
[5] S. Kotake, N. Udagawa, N. Takahashi, et al., IL-17 in synovial fluids from patients with rheumatoid arthritis is a potent stimulator of osteoclastogenesis, J. Clin. Investig. 103 (9) (1999) 1345–1352.
[6] P. Liu, S. Lee, J. Knoll, et al., Loss of menin in osteoblast lineage affects osteocyte–osteoclast crosstalk causing osteoporosis, Cell Death Differ. 24 (4) (2017) 672–682.
[7] H. Tao, G. Ge, W. Li, et al., Dysimmunity and inflammatory storm: watch out for bone lesions in COVID-19 infection, Med. Hypotheses 145 (2020) 110332.
[8] X. Wu, X. Feng, Y. He, et al., IL-4 administration exerts preventive effects via suppression of underlying inflammation and TNF-α-induced apoptosis in steroid-induced osteonecrosis, Osteoporos. Int. 27 (5) (2016) 1827–1837.
[9] L. Di Filippo, A.M. Formenti, P. Rovere-Querini, et al., Hypocalcemia is highly prevalent and predicts hospitalization in patients with COVID-19, Endocrine. 68 (3) (2020) 475–478.
[10] L. Bao, W. Deng, B. Huang, et al., The pathogenicity of SARS-CoV-2 in hACE2 transgenic mice, Nature. 583 (7818) (2020) 830–833.
[11] B. Israelow, E. Song, T. Mao, et al., Mouse model of SARS-CoV-2 reveals inflammatory role of type I interferon signaling, J. Exp. Med. 217 (12) (2020).
[12] 034860 - B6.Cg-Tg(K18-ACE2)2Prlmn/J. *K18-hACE2 mice.*
[13] M.D. Johansen, A. Irving, X. Montagutelli, et al., Animal and translational models of SARS-CoV-2 infection and COVID-19, Mucosal Immunol. 13 (6) (2020) 877–891.
[14] P. Zhou, X.-L. Yang, X.-G. Wang, et al., A pneumonia outbreak associated with a new coronavirus of probable bat origin, Nature. 579 (7798) (2020) 270–273.
[15] J. Damas, G.M. Hughes, K.C. Keough, et al., Broad host range of SARS-CoV-2 predicted by comparative and structural analysis of ACE2 in vertebrates, Proc. Natl. Acad. Sci. 117 (36) (2020) 22311.
[16] B. McCray Paul, L. Pewe, C. Wohlford-Lenane, et al., Lethal infection of K18-hACE2 mice infected with severe acute respiratory syndrome coronavirus, J. Virol. 81 (2) (2007) 813–821.
[17] E.S. Winkler, A.L. Bailey, N.M. Kafai, et al., SARS-CoV-2 infection of human ACE2-transgenic mice causes severe lung inflammation and impaired function, Nat. Immunol. 21 (11) (2020) 1327–1335.
[18] C.K. Yinda, J.R. Port, T. Bushmaker, et al., K18-hACE2 mice develop respiratory disease resembling severe COVID-19, PLoS Pathog. 17 (1) (2021), e1009195.

[19] L.A. Santry, J.C. Ingrao, D.L. Yu, et al., AAV vector distribution in the mouse respiratory tract following four different methods of administration, BMC Biotechnol. 17 (1) (2017) 43.
[20] J.B. Case, A.L. Bailey, A.S. Kim, R.E. Chen, M.S. Diamond, Growth, detection, quantification, and inactivation of SARS-CoV-2, Virology. 548 (2020) 39–48.
[21] E.A. Nunamaker, R.J. Anderson, J.E. Artwohl, A.V. Lyubimov, J.D. Fortman, Predictive observation-based endpoint criteria for mice receiving total body irradiation, Comp. Med. 63 (4) (2013) 313–322.
[22] F.C. Hankenson, N. Ruskoski, M. van Saun, G.-S. Ying, J. Oh, N.W. Fraser, Weight loss and reduced body temperature determine humane endpoints in a mouse model of ocular herpesvirus infection, J. Am. Assoc. Lab. Anim. Sci. 52 (3) (2013) 277–285.
[23] E.D. Olfert, D.L. Godson, Humane endpoints for infectious disease animal models, ILAR J. 41 (2) (2000) 99–104.
[24] M.H. Ullman-Culleré, C.J. Foltz, Body condition scoring: a rapid and accurate method for assessing health status in mice, Lab. Anim. Sci. 49 (3) (1999) 319–323.
[25] J. Zheng, L.-Y.R. Wong, K. Li, et al., COVID-19 treatments and pathogenesis including anosmia in K18-hACE2 mice, Nature. 589 (7843) (2021) 603–607.
[26] S.A. Lloyd, C.H. Lang, Y. Zhang, et al., Interdependence of muscle atrophy and bone loss induced by mechanical unloading, J. Bone Miner. Res. 29 (5) (2014) 1118–1130.
[27] Learn What Osteoporosis Is and What It's Caused by. National Osteoporosis Foundation. www.nof.org, accessed September 16, 2021.
[28] B. Hu, S. Huang, L. Yin, The cytokine storm and COVID-19, J. Med. Virol. 93 (1) (2021) 250–256.
[29] F. La Rosée, H.C. Bremer, I. Gehrke, et al., The Janus kinase 1/2 inhibitor ruxolitinib in COVID-19 with severe systemic hyperinflammation, Leukemia. 34 (7) (2020) 1805–1815.
[30] B. Liu, M. Li, Z. Zhou, X. Guan, Y. Xiang, Can we use interleukin-6 (IL-6) blockade for coronavirus disease 2019 (COVID-19)-induced cytokine release syndrome (CRS)? J. Autoimmun. 111 (2020) 102452.
[31] S.H. Nile, A. Nile, J. Qiu, L. Li, X. Jia, G. Kai, COVID-19: pathogenesis, cytokine storm and therapeutic potential of interferons, Cytokine Growth Factor Rev. 53 (2020) 66–70.
[32] D. Ragab, H. Salah Eldin, M. Taeimah, R. Khattab, R. Salem, The COVID-19 cytokine storm; what we know so far, Front. Immunol. 11 (2020), 01446, https://doi.org/10.3389/fimmu.2020.01446.
[33] J. Wang, M. Jiang, X. Chen, L.J. Montaner, Cytokine storm and leukocyte changes in mild versus severe SARS-CoV-2 infection: review of 3939 COVID-19 patients in China and emerging pathogenesis and therapy concepts, J. Leukoc. Biol. 108 (1) (2020) 17–41.
[34] J. Gao, H. Mei, J. Sun, et al., Neuropilin-1 Mediates SARS-CoV-2 Infection in Bone Marrow-derived Macrophages, Cold Spring Harbor Laboratory, 2021.